stellarator news

An international journal of news from the stellarator community

Editor: James A. Rome Issue 162 June 2018
E-Mail: James.Rome@stelnews.info Phone: +1 (865) 482-5643
On the Web at https://stelnews.info

Managing leading edges in the Wendelstein 7-X divertor

1. The W7-X divertor

In Wendelstein 7-X (W7-X), the magnetic islands occurring naturally at magnetic surfaces with rational values of the rotational transform are used for divertor operation [1]. In such an island divertor, the islands are intersected by target plates. Due to the low magnetic shear in W7-X, rather long paths (in the range 150–400 m) along the magnetic field within an island may be achieved before a field line intersects a target plate in spite of the small direct distance between the X points of the island chain and the target plates [2].

The target plates are three-dimensionally shaped to ensure that the thermal load does not exceed the design value of 10 MW/m^2 locally, using a simple field line diffusion model (as described, e. g., in Ref. [3]) with an assumed diffusion coefficient of 1 m^2/s, for any of nine reference magnetic vacuum configurations. The resulting target plates intersect the magnetic field at angles of 1°–3° in those regions where the heat flux along the magnetic field is largest, thus limiting the thermal load to the targets as required.

Under the aforementioned assumptions, the maximal heat load onto surfaces oriented perpendicular to the magnetic field (such as leading edges) is expected to be of order 200 MW/m^2. Therefore, the height of leading edges must be minimized. The locations of the regions of highest thermal load (strike lines) on the target plates in reality may deviate from the modeling due to deviations of the magnetic field from the underlying vacuum configurations (finite-beta effects, additional driven plasma currents, use of different magnetic configurations), but also due to particle drifts which are not taken into account in the model. Therefore, the design of the targets was chosen to minimize leading edges between target elements everywhere on the target surface by introducing steps and slight inclinations at gaps, so that leading edges are shadowed by the adjacent target element.

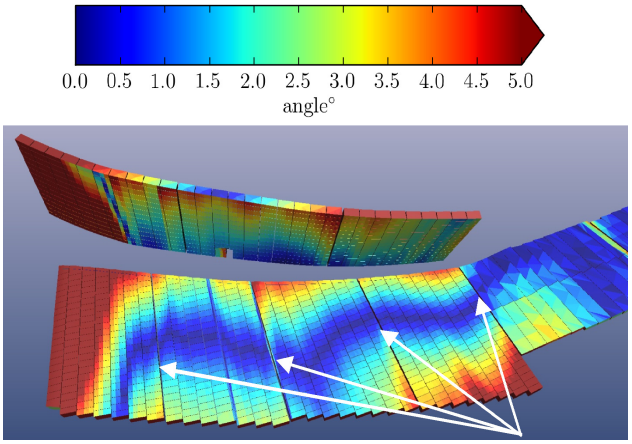

Fig.1. Incident angle of the magnetic field on a portion of the target plates. The larger gaps of 5 ± 1.5 mm between adjacent target elements are indicated by arrows. The direction of incidence is not shown, but the poloidal "watershed" with an angle of incidence of 0° is clearly visible along most of the horizontal target plates. The direction of incidence changes sign when crossing the poloidal watershed (see Fig. 2).

In this issue . . .

Due to technical boundary conditions, there exist gaps of up to 7 mm between target modules in some locations, and there is a poloidal watershed in some areas of the targets (see Fig. 1). The watershed is defined as the line where the angle of incidence of the magnetic field on the target surface changes sign, here between the torus outboard and inboard sides of the target plates.

2. Requirements for accuracy during divertor assembly

If there is a gap between target elements crossing the watershed, the potential leading edge will change side between the two target elements at the watershed, and the target elements must be inclined relative to each other in order to achieve shadowing on both sides of the watershed (Fig. 2). However, the position of the watershed changes by several centimeters between magnetic configurations, such that a compromise for the design of the target elements had to be found, which required a relative positioning accuracy of 0.2 mm between adjacent target modules.

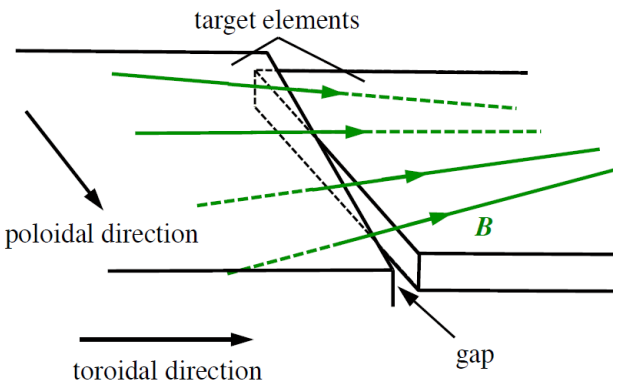

Fig. 2. Schematic view of the relative inclination of two target elements with a gap that might cause leading edges to be exposed to heat flux from the plasma along the magnetic field lines. In this case, the direction of incidence of the magnetic field reverses along the gap, and the two target elements are inclined in such a way that the leading edge is always shadowed by the adjacent target element. Since the point of field inclination reversal shifts poloidally for different magnetic configurations, and since the target elements are positioned within a given accuracy, the shadowing will not be perfect for all configurations.

In order to gain experience in W7-X divertor operation before the installation of the water-cooled high heat flux (HHF) divertor, which will be capable of steady-state high-power discharges, W7-X will first be operated with an inertially cooled test divertor unit (TDU) with the same surface shape as the HHF divertor. With this TDU, the power input will be initially limited to 80 MJ per discharge (e. g., 8 MW ECRH for 10 s). As (1) the alignment of the divertor frames to the originally defined relative accuracy of 0.2 mm requires a significant amount of assembly time, (2) in contrast to later HHF divertor operation, stationary target temperatures will not be reached during TDU operation, and (3) only a limited number of magnetic configurations is envisaged for the TDU operation phase, we decided to reassess the potential impact of leading edges.

Rather than avoiding leading edges with an effective height above 0.2 mm everywhere on the target surface, we chose to focus on the locations of the strike lines (according to the field line diffusion model) and on magnetic configurations selected for high-power operations in the TDU phase. We would allow for larger tolerances in the assembly of the targets but would measure the resulting step height along the gaps between target elements. We would estimate the expected carbon evaporation rate due to the as-built steps for the specified magnetic configurations and would realign the targets if the estimated carbon evaporation was so large that radiation collapses would likely limit the operation of W7-X.

3. Approach to assess the impact of leading edges

The goal for positioning the TDUs was to avoid steps between adjacent target elements that might cause such high carbon evaporation rates due to plasma hitting leading edges that operation in OP1.2 would be severely limited. We use a carbon evaporation rate given in Ref. [4].

In a finite element method (FEM) model of a leading edge, the local temperature is obtained by balancing the incident power onto the target surface P with radiation, heat conduction into the bulk graphite, and sublimation. The resulting temperature field is used to calculate the local evaporation rate per unit length of the leading edge, which depends on the time from the start of the discharge t, on P, and on the height of the leading edge h_{LE} (taking into account the gap width, the incident angle of the magnetic field, and a possible step between the target surfaces on both sides of the gap). By integrating this local evaporation rate along a gap, where P and h_{LE} will vary along the gap, a time-dependent total evaporation rate for a specific gap and a specific magnetic configuration is calculated.

The FEM model is used to create a table of local evaporation rates for t in the range 0–40 s, P in the range 10–230 MW/m^2, and h_{LE} in the range 0–3 mm. This table can then be used to quickly compute, by appropriate interpolation, the local evaporation rates for any given set of (t, P, h_{LE}) values along the gaps between divertor modules.

A simple estimate of the local power density to a target surface is provided by the "field line diffusion" model: Magnetic field line tracing is started at arbitrary points slightly inside the last closed magnetic flux surface, and after some "free path" length, a random step perpendicular

to the magnetic field is added. This corresponds to test particles moving parallel to the magnetic field and undergoing a diffusion perpendicular to the magnetic field [3]. The parameters of this process are chosen to reflect the ratio of parallel to perpendicular transport in the plasma edge. In the end, all the tracing paths will intersect some wall component. The density of hit points on the target surface is then a measure for the power density in this location for the underlying magnetic configuration. The incident power density can also be computed by more sophisticated models such as the EMC3/Eirene code [5, 6], which is, however, significantly more computationally expensive.

Both approaches were used, but most calculations were performed with field line diffusion.

In order to obtain good spatial resolution along the gaps between target elements, we subdivided the target surface into pieces with a length of 5 mm along the gap and 40 mm perpendicular to the gap. To achieve good statistics then requires the tracing of $O(10^6)$ test particles.

In most areas, the magnetic field intersects the target surface under a small angle α. The incident power density parallel to the magnetic field is therefore larger by a factor of $1/\sin\alpha$. A leading-edge hit under an angle γ is therefore exposed to a power density larger by a factor $\sin\gamma/\sin\alpha$ than the power density to the target surface, and γ is typically much larger than α. We therefore obtain the power density P to the leading edge from the power density to the local target surface P_{surf} from field line diffusion or EMC3/Eirene as

$$P = P_{\mathrm{surf}} \frac{\sin\gamma}{\sin\alpha}.$$

As examples, we show in Fig. 3 surface loads P_{surf} and resulting loads P on leading edges at the gap between two modules of the horizontal target for two different magnetic configurations ("scraper element mimic configurations" for a toroidal plasma current of 0 and of 43 kA, see Ref. [7]).

The outlined procedure for calculating the projected power density to the face of a leading edge might appear to be unnecessarily complicated. Obviously, it would be more straightforward to count the hits to the face of a leading edge directly in the field line diffusion model. However, since this face area is very small for the design case, an even higher number of test particles would be required to achieve good statistics. During the optimization procedure (see Section 4), the step height between adjacent divertor modules is varied, which would require a multiple repetition of the field line diffusion calculation for different step heights. In our implementation, the local power density P_{surf} as a function of position along the gap remains independent of the step height and depends only on the choices of gap and magnetic configuration. The total evaporation rate along the gap $e_{\mathrm{tot}}(t)$ can then quickly be evaluated from the table of local evaporation rates, as outlined above.

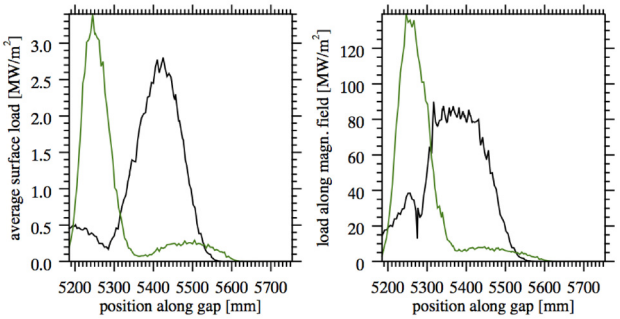

Fig. 3. Left: surface power loads P_{surf} to the target surfaces adjacent to the gap between target modules 3h and 4h, as calculated in a field line diffusion model, for two magnetic configurations (black and green); right: resulting power loads P_{ll} to a leading edge. The abscissa coordinate is the length along the gap, with the major radius of the inboard end of the gap as an offset.

After installation of each TDU in the W7-X plasma vessel, the step heights were measured with a dial gauge at 3–4 positions along the gap between any two adjacent target modules. The deviation of the measured steps from the design values was then interpolated to obtain the as-built step height along the gap. An example is shown in Fig. 4.

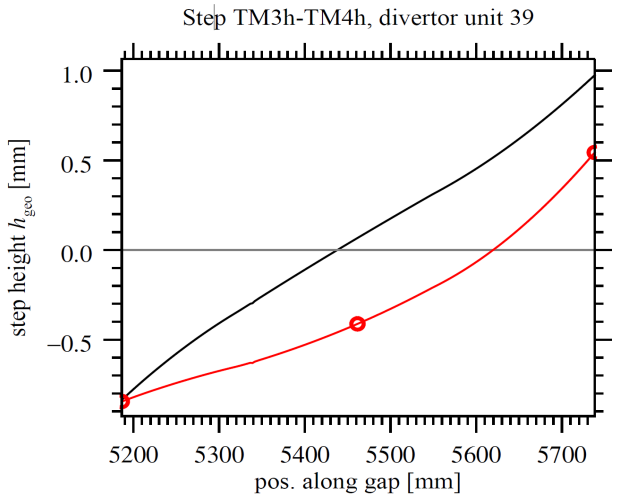

Fig. 4. Step height of target module 4h above target module 3h in divertor unit 39 design (black) versus as-built (red). The three measurements along the gap are marked by circles. According to the design, the edges of the two target modules are tilted relative to each other, as shown in Fig. 2.

The height of the leading edge can now be calculated for a given magnetic configuration from the as-built step height and from the magnetic field vector and the surface normal vector for each point along the target edge.

Likewise, for each point along the target edge the incident power density P_{LE} to the leading edge can be calculated for each magnetic configuration from $P_{||}$ and from the magnetic field vector and the normal vector on the face of the leading edge.

Finally, the local evaporation rate along the gap and the total evaporation rate for the entire gap $e_{tot}(t)$ can be calculated (see Fig. 5).

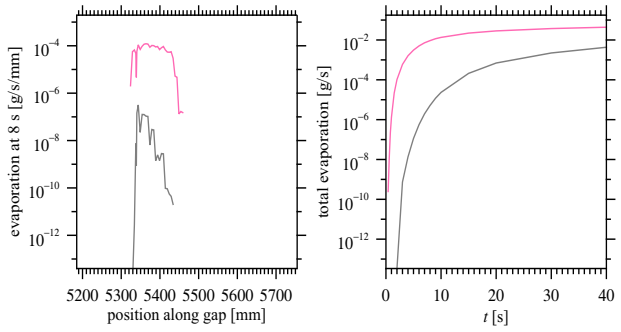

Fig. 5. Left: Local evaporation rate after 8 s, corresponding to the surface power shown in Fig. 3. Of the two magnetic configurations, only for the one shown in black in Fig. 3, and only at the leading edge at target module 3h are the temperatures high enough to yield significant carbon evaporation after 8 s. Whereas in the CAD alignment (gray curves),
the evaporation rate is still tolerable at this time of the discharge, it becomes three orders of magnitude larger for the as-built alignment (pink curves). Right: Time evolution of the total evaporation rate e_{tot}, integrated along the entire gap.

4. Optimizing the steps between divertor modules

In the framework of our model, we calculated evaporation rates for the as-built state of all gaps between target modules in all ten test divertor units of W7-X, as described in Section 3. We did this for a number of magnetic configurations, which were considered relevant for the TDU operation phase.

Our criterion was to avoid a situation where the operation of W7-X would be limited by strong carbon evaporation from leading edges. With a plasma volume of roughly 30 m^3 and an assumed plasma density of at least 2×10^{19} m^{-3}, we obtain an overall particle content of 6×10^{20}. Therefore, the plasma should certainly not contain more than 10^{20} carbon ions, corresponding to 2×10^{-3} g. Considering the uncertainties of modeling as an order of magnitude, a carbon evaporation rate of 10^{-4} g/s will be regarded as a second critical threshold.

As mentioned in Section 2, precise alignment of most of the target modules would require a significant amount of assembly time. However, one type of target module can be re-aligned within its divertor frame without major time effort. This type of target module (TM5h1) happens to have a critical gap toward TM4h, where a large carbon evaporation rate is likely in case of misalignment. Our compromise for the assembly strategy therefore was to plan for a realignment of TM5h1, in all ten divertor units, whereas we would monitor all other gaps between target modules and take action only if our model would indicate a particularly high evaporation rate at such a location.

Once the as-built step heights between the target modules 4h, 5h1 and 5h2 had been measured in a divertor unit, the necessary shifts were calculated. TM5h1 is positioned into the divertor frame by means of two fitted brackets and one fitted bushing. For the new alignment, TM5h1 was removed, new brackets and a new bushing were manufactured to the newly calculated measures, the target module was reinstalled, and the step heights were measured again. A typical accuracy of 0.2 mm was thus achieved.

The realignment changes the step heights at the gaps between TM4h and TM5h1, and between TM5h1 and TM5h2. In order to find the optimum alignment of TM5h1, the step heights at the inboard end and at the outboard end of the gap are represented by a pair of values (h_1, h_2), which are then varied. For each realization of (h_1, h_2), the new total evaporation rates after 8 s at the two gaps in question are calculated, and a weighted average of the evaporation rates is taken for the magnetic configurations considered relevant. This result is then minimized by varying the parameters (h_1, h_2).

In fact, we perform a stochastic optimization; that is, we optimize the evaporation rate for Gauss distributions of shifts around each pair of nominal (h_1, h_2) values, with standard deviations of 0.2 mm. By this procedure we avoid choosing a narrow minimum which will most probably not be realized due to the finite accuracy of the realignment.

In the most severe case, the sum of the weighted averages of the evaporation rate from both gaps would be reduced from 0.27 g/s (initial installation) to 6.7×10^{-4} g/s (re-aligned).

5. Results of test divertor assembly

The resulting carbon evaporation rates from our model for each gap between target modules and for the steps between certain target elements are summarized in Fig. 6. The value for each gap is the weighted average of the

results for different magnetic configurations, as considered appropriate for the TDU operation phase of W7-X. In many cases, only one or two magnetic configurations contribute significantly; the values for such configurations could be higher by a factor of ~10.

We note that the critical values 10^{-4} g/s and 2×10^{-3} g/s (gray horizontal lines in Fig. 6) are already reached or exceeded at several gaps. The limit of 2×10^{-3} g/s was only exceeded at gap 6, which is between the target modules 4h and 5h1, before the realignment described in section 4 (full symbols), and at gap no. 3 in one case (full red square). The latter case concerned one target element with inlays for the investigation of plasma-wall interactions, which was also realigned. In all cases, the modeled evaporation rates after the realignment (open symbols) did not exceed the level of 2×10^{-3} g/s.

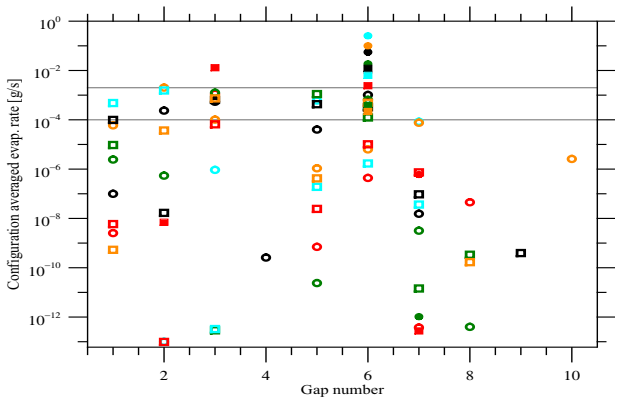

Fig. 6. Carbon evaporation rates $e_{tot}(t = 8\ s)$ for 10 MW heating power, weighted average for magnetic configurations relevant for the TDU operation phase, as calculated in our model, for the step heights measured after the integration of the TDUs into W7-X. The gaps are numbered in toroidal order for the horizontal target modules within one divertor unit, and the colors indicate different machine modules. Symbol code — circles: upper divertor units; squares: lower divertor units; full symbols: before realignment; open symbols: after realignment, or no realignment. Horizontal gray lines: indication of the thresholds 10^{-4} g/s and 2×10^{-3}g/s.

An extended version of this report is in preparation for publication as a journal article.

This work has been carried out within the framework of the EUROfusion Consortium and has received funding from the EURATOM research and training programme 2014–2018 under grant agreement no. 633053. The views and opinions expressed herein do not necessarily reflect those of the European Commission.

References

[1] H. Renner, J. Boscary, V. Erckmann, H. Greuner, H. Grote, J. Sapper, E. Speth, F. Wesner, M. Wanner, and W7-X Team. "The capabilities of steady state operation at the stellarator W7-X with emphasis on divertor design." Nucl. Fusion **40**(6) 1083–1093, June 2000.

[2] Y. Feng, C. D. Beidler, J. Geiger, P. Helander, H. Hölbe, H. Maassberg, Y. Turkin, D. Reiter, and W7-X Team. "On the W7-X divertor performance under detached conditions." Nucl. Fusion **56**(12) 126011, December 2016.

[3] S. A. Bozhenkov, J. Geiger, M. Grahl, J. Kißlinger, A.Werner, and R. C.Wolf. "Service-oriented architecture for scientific analysis at W7-X. An example of a field line tracer." Fusion Eng. and Des. **88**(11) 2997–3006, November 2013.

[4] V. Philipps, U. Samm, M. Z. Tokar', B. Unterberg, A. Pospieszczyk, and B. Schweer. "Evidence of hot spot formation on carbon limiters due to thermal electron emission." Nucl. Fusion **33**(6) 953–961, June 1993.

[5] Y. Feng, F. Sardei, J. Kisslinger, P. Grigull, K. McCormick, and D. Reiter. "3D edge modeling and island divertor physics." Contrib. Plasma Phys. **44**(1–3) 57–69, April 2004. Special Issue: Proceedings of 9th Workshop on Plasma Edge Theory in Fusion Devices (PET-9), September 3–5, 2003, University of California in San Diego, USA.

[6] P. Sinha, H. Hölbe, T. S. Pedersen, S. Bozhenkov, and W7-X Team. "Numerical studies of scrape-off layer connection length in Wendelstein 7-X." Nucl. Fusion **58**(1) 016027, January 2018.

[7] H. Hölbe, T. Sunn Pedersen, J. Geiger, S. Bozhenkov, R. König, Y. Feng, J. Lore, A. Lumsdaine, and Wendelstein 7-X Team. "Access to edge scenarios for testing a scraper element in early operation phases of Wendelstein 7-X". Nucl.Fusion **56**(2) 026015, February 2016.

Michael Endler for the W7-X Team
Max-Planck-Institut für Plasmaphysik
D-17491 Greifswald, Germany
E-mail: michael.endler@ipp.mpg.de